PCCP

ROYAL SOCIETY OF CHEMISTRY

PAPER

View Article Online
View Journal | View Issue

Cite this: *Phys. Chem. Chem. Phys.*, 2023, **25**, 8524

An automated reaction route mapping for the reaction of NO and active species on Ag_4 clusters in zeolites†

Shunsaku Yasumura, [a] Taisetsu Kato,[a] Takashi Toyao, [a] Zen Maeno [b] and Ken-ichi Shimizu *[a]

A computational investigation of the catalytic reaction on multinuclear sites is very challenging. Here, using an automated reaction route mapping method, the single-component artificial force induced reaction (SC-AFIR) algorithm, the catalytic reaction of NO and OH/OOH species over the Ag_4^{2+} cluster in a zeolite is investigated. The results of the reaction route mapping for H_2 + O_2 reveal that OH and OOH species are formed over the Ag_4^{2+} cluster *via* an activation barrier lower than that of OH formation from H_2O dissociation. Then, reaction route mapping is performed to examine the reactivity of the OH and OOH species with NO molecules over the Ag_4^{2+} cluster, resulting in the facile reaction path of HONO formation. With the aid of the automated reaction route mapping, the promotion effect of H_2 addition on the SCR reaction was computationally proposed (boosting the formation of OH and OOH species). In addition, the present study emphasizes that automated reaction route mapping is a powerful tool to elucidate the complicated reaction pathway on multi-nuclear clusters.

Received 12th October 2022,
Accepted 10th February 2023

DOI: 10.1039/d2cp04761f

rsc.li/pccp

1. Introduction

Automated reaction route mapping is considered a powerful method for elucidating the mechanism of chemical reactions.[1–10] Maeda *et al.* developed an artificial force-induced reaction (AFIR) method implemented in the global reaction route mapping (GRRM) program as an efficient reaction path-searching method; additionally, they demonstrated the rational design of chemical reactions in homogeneous systems.[11–16] Investigating the reaction mechanism over multinuclear clusters in heterogeneous systems is challenging[17–21] because various active sites are present in one cluster (*e.g.*, on-top, bridge, and hollow sites) and their shapes change during the reaction.[22–25] Thus, the exploration of the reaction mechanism over the clusters, based on transition state calculations, focuses typically only on some critical steps expected from previous results and experiences, which hinders the identification of more plausible reaction pathways.[26–33] Gao *et al.* employed the AFIR method to investigate the structural transformation of neutral Au_x clusters (x = 3–12) induced by O_2 adsorption and reported that the transformation of Au clusters was promoted by O_2 adsorption.[34] Similarly, Iwasa *et al.* investigated the relationship between the structural transformation of a Cu_{13} cluster and NO dissociation using the AFIR method.[35] Although the aforementioned studies reveal the nature of metal clusters and adsorbed molecules by the AFIR method, the detailed reaction mechanism in the catalytic processes over metal clusters has not been reported.

Ag-loaded Al_2O_3 and Ag-exchanged zeolites have been studied for the selective catalytic reduction of NO to N_2 (SCR).[36–39] Interestingly, adding a small amount of H_2 improved the SCR performance of these catalysts; many researchers have intensively studied the reaction mechanism of H_2-assisted SCR on Ag-loaded Al_2O_3 and unraveled that the oxidized Ag species was promoted to be reduced into the metallic state by H_2.[40–48] In the case of Ag-exchanged zeolite, in the presence of H_2, the formed $Ag_n^{\delta+}$ clusters improved the SCR performance.[49–53] Shibata *et al.* performed UV-vis and XAS measurements, which revealed that the average structure of the formed cluster in the zeolite was Ag_4^{2+}.[54] Using *in situ* IR measurements, Shimizu *et al.* reported that the formed $Ag_n^{\delta+}$ cluster activates O_2 and H_2 to yield OOH species that are responsible for the drastic improvement in ammonia- (NH_3–) and hydrocarbon-(HC-) SCR performance.[52,55] For decades, numerous experimental[50–52,55,56] and theoretical[53] investigations have been reported on the characterization of active Ag clusters and plausible SCR mechanisms. However, these studies still lack a molecular-level understanding of the reaction pathways based on computational techniques.

In this study, using automated reaction route mapping, the reaction of H_2 and O_2 was investigated over Ag_4^{2+} clusters

[a] *Institute for Catalysis, Hokkaido University, N-21, W-10, Sapporo, 001-0021, Japan. E-mail: kshimizu@cat.hokudai.ac.jp*
[b] *School of Advanced Engineering, Kogakuin University, Tokyo, 192-0015, Japan*

† Electronic supplementary information (ESI) available. See DOI: https://doi.org/10.1039/d2cp04761f

confined in CHA zeolite (a relatively small number of atoms are required to describe its periodic model). The formation of OOH and OH species from H_2 + O_2 requires a lower activation barrier than OH formation from H_2O dissociation over the Ag_4^{2+} cluster. Subsequently, the reactivity of NO with the active species formed on Ag_4^{2+} was assessed. The results indicated that minimal activation barrier was required to produce the HONO intermediate, which then migrated into the Brønsted acid sites to give N_2 + H_2O *via* reaction with NH_3 (discussed in our previous reports[57]). Similarly, the NO + H_2 reaction required a relatively high activation barrier to produce NH_3, thus indicating that NO preferentially reacts with the active species, OH, and OOH species on the Ag_4^{2+} cluster. The present study demonstrates the effective use of an automated reaction path-searching method to explore catalytic reactions in multinuclear clusters.

2. Computational details

Spin-polarized density functional theory (DFT) calculations were performed using the Vienna Ab initio Simulation Package (VASP).[58,59] In particular, the projected augmented wave (PAW) method[60,61] was employed for the Kohn–Sham equations[62,63] with a plane-wave energy cutoff of 400 eV. The generalized gradient approximated Perdew–Burke–Ernzerhof (GGA-PBE) functional[64] was employed to describe the electron exchange-correlation. The Brillouin zone sampling was restricted to the Γ point (convergence tests of cutoff energy and k-point mesh are shown in Table S1 and S2, ESI†).[65] van der Waals interactions were considered using the dispersion-corrected DFT-D3 (BJ) method.[66,67] The periodic model of the CHA zeolite, utilized as the model zeolite for reducing the computational cost for the reaction mapping, was obtained from the International Zeolite Association (IZA) database (a = b = 13.7 Å, c = 14.8 Å, α = β = 90.0°, and γ = 120°).[68] The lattice constants were fixed at the initial values during the calculations (comparison before/after the optimization of the lattice constants is shown in Table S3, ESI†). CHA zeolite is composed of only one crystallographically inequivalent T site,[69] and the third-nearest-neighbor in a six-membered ring site (6MR3NN site) in CHA was considered a model paired Al site in this study (Fig. 1).[26,70,71] Reaction route mapping was performed using the single-component artificial force induced reaction (SC-AFIR) method, as implemented in the GRRM17 program.[16] In this method, a structural deformation is induced by pushing or pulling a pair of target atoms with the applied artificial force using the following AFIR function.[16]

$$F^{\mathrm{AFIR}}(Q) = E(Q) + \rho\alpha\frac{\sum_{i\in A}\sum_{j\in B}\omega_{ij}\mathrm{r}_{ij}}{\sum_{i\in A}\sum_{j\in B}\omega_{ij}}$$

$E(Q)$ represents the potential energy surface (PES) of geometrical parameters Q. In the second term, the artificial force is applied to the system, and the strength of the artificial force is controlled by α, where ρ is set to either 1 or −1. r_{ij} represents the interatomic distance of atoms i and j in fragments A and B, respectively. The weight ω_{ij} is described as,

$$\omega_{ij} = \left[\frac{\mathrm{R}_i + \mathrm{R}_j}{\mathrm{r}_{ij}}\right]^6$$

where R_i and R_j represent each covalent radius.

A model collision energy parameter of 1000 kJ mol^{-1} was used for all calculations. The obtained AFIR path was subsequently optimized by the locally updated plane (LUP) method to obtain the approximate equilibrium structures (EQs) and path top (PT) points, which were subsequently re-optimized by the following intrinsic reaction coordinate (IRC) calculation to determine the transition state (TS) structures and their connectivity.[72] The structures are treated to be optimized when the difference in their electronic energies, the RMS error in interatomic distances, and the maximum error in interatomic distances are all smaller than 6.0 kJ mol^{-1}, 3%, and 6%, respectively. Only a positive force was applied to the SC-AFIR calculations. Reactants in the gas phase (H_2, O_2, and NO molecules) of the initial structures were considered the target atoms of the SC-AFIR algorithm. During the calculations, the positions of the atoms in the zeolite framework were fixed at the initial positions, except for the Al atoms, the Si atoms around the Al atoms, and the O atoms connected to the Al and Si atoms (Fig. 1b).[73] All the structures predicted in this study can be found in the ESI.†

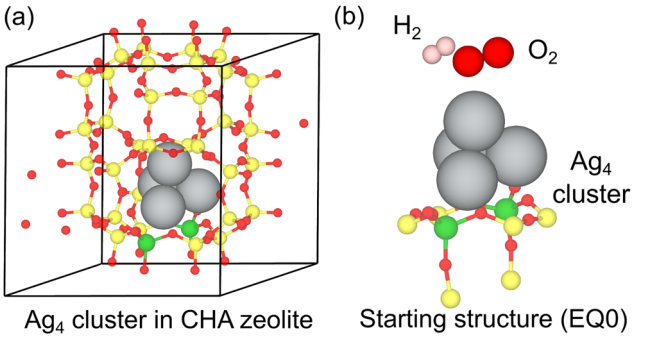

Fig. 1 (a) Utilized periodic model of CHA zeolite including the Ag_4 cluster and (b) the starting structure (EQ0) for the reaction route mapping with the SC-AFIR method.

3. Results and discussion

3.1 Reaction route mapping of the H_2 + O_2 reaction to produce an OH group over the Ag_4 cluster in CHA zeolite

Our group previously reported the mechanism of NH_3–SCR, wherein the OH species bound to transition metal cations oxidizes NO into HONO species ($M^{n+}(OH)$ + NO → $M^{(n-1)+}$ + HONO; M^{n+} describes metal cations) that then migrate into Brønsted acid sites (BAS) to form H_2O and NO^+ species (HONO + $H^+O_z^-$ → $NO^+O_z^-$ + H_2O; $H^+O_z^-$ represents BAS) that easily react with NH_3 to produce N_2 and H_2O ($NO^+O_z^-$ + NH_3 → $H^+O_z^-$ + N_2 + H_2O).[57,74–77] Thus, the generation of OH groups on active metal cations is a crucial step in the SCR reaction.

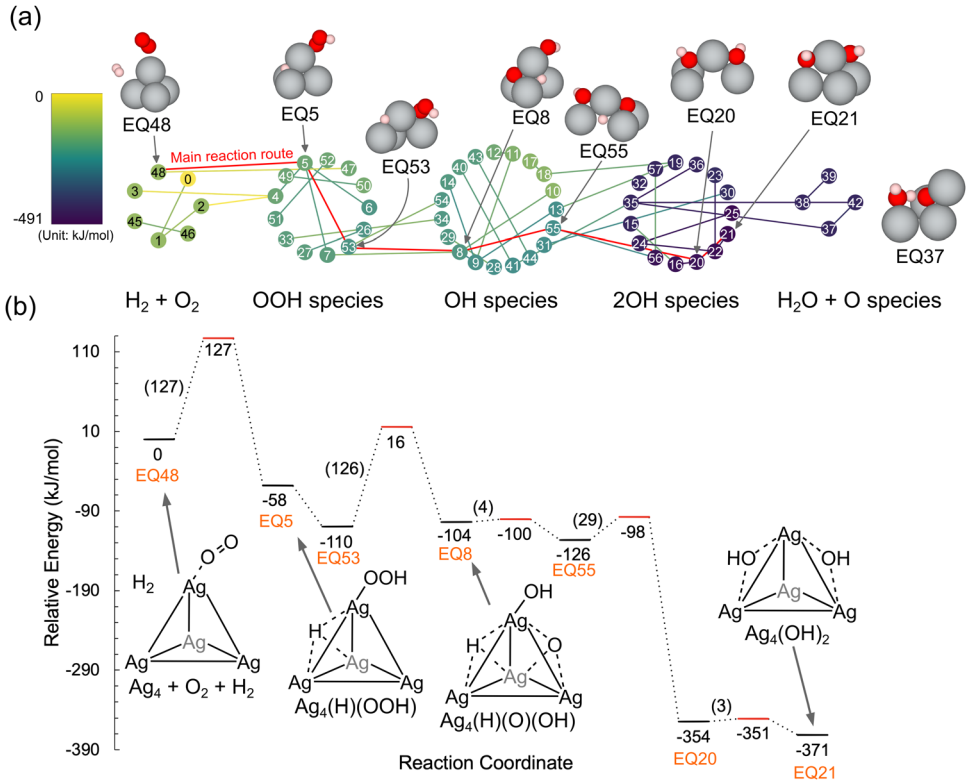

Fig. 2 (a) Reaction route network for $H_2 + O_2$ on a Ag_4 cluster in CHA zeolite. Nodes and edges describe obtained structures and paths connecting them (TS and PT, determined by GRRM program[16]). The color of the nodes and edges represents the relative energy (the color bar is shown on the left side). The representative structures are displayed together (only the Ag_4 cluster and reactants are shown for clarity). (b) Energy profile for the main reaction route toward EQ21. The relative energies of each structure and the activation barriers are shown below the bar and in brackets, respectively. Schematic views of the structures are displayed together.

Here, the $H_2 + O_2$ reaction was explored to assess the feasibility of generating OH groups on the $Ag_n^{\delta+}$ cationic cluster. Shibata *et al.* reported that in the presence of H_2, Ag_4^{2+} clusters were generated within the zeolite framework and acted as active sites for the SCR reaction.[54] Encouraged by their study, the Ag_4^{2+} cluster at the 2Al site was used as the initial structure. Fig. 1a shows the periodic model of CHA zeolites obtained from the IZA database. In this study, two *T* sites in the six-membered ring of CHA were replaced by Al.[70] As a starting structure, O_2 and H_2 molecules were added to the periodic model, including the Ag_4^{2+} cluster (Fig. 1b), and the reaction route was explored by the SC-AFIR method. Fig. 2a shows the results of the reaction route mapping, and the relative energies along the main reaction coordinates are shown in Fig. 2b. 57 of the structures, which showed different shapes of Ag_4^{2+} clusters, and 57 of their connections (TS and PT) were found by the aid of the SC-AFIR method. In the first step, H_2 molecules were dissociated to give OOH species and H atoms on the Ag_4 cluster *via* an activation barrier (*Ea*) of 127 kJ mol^{-1}. Sawabe *et al.* also performed DFT calculations to reveal that OOH species on the Ag_4^{2+} cluster are potential active species for the SCR reaction while H_2 dissociation took place as the first step in their reaction path (activation barrier of OOH formation was not shown).[53] Next, the formed OOH species dissociated into OH and O species on the cluster with an *Ea* of 125 kJ mol^{-1}. Subsequently, the O atom combined with the H atom to give another OH species *via* low *Ea*s (4, 29, and 3 kJ mol^{-1}) with an exothermicity of 371 kJ mol^{-1}. The dissociation of H_2O molecules to form OH species on the Ag_4 cluster was also examined (Fig. 3). The results revealed that the formation of OH species from $H_2 + O_2$ required a lower *Ea* than the H_2O

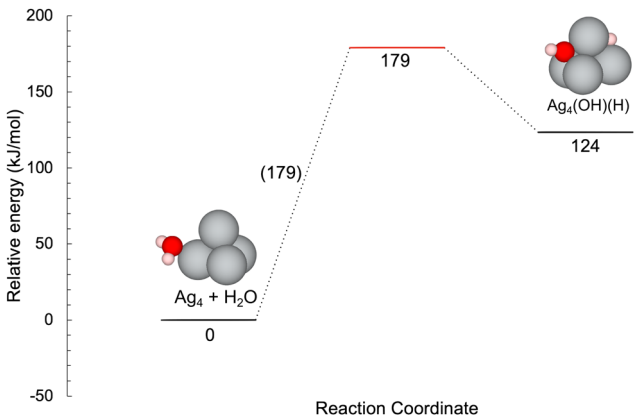

Fig. 3 Energy profile for H_2O dissociation reaction to yield OH species and a H atom over a Ag_4 cluster. The relative energies of each structure and the activation barriers are shown below the bar and in brackets, respectively. The structures are displayed together (only the Ag_4 cluster and reactants are shown for clarity).

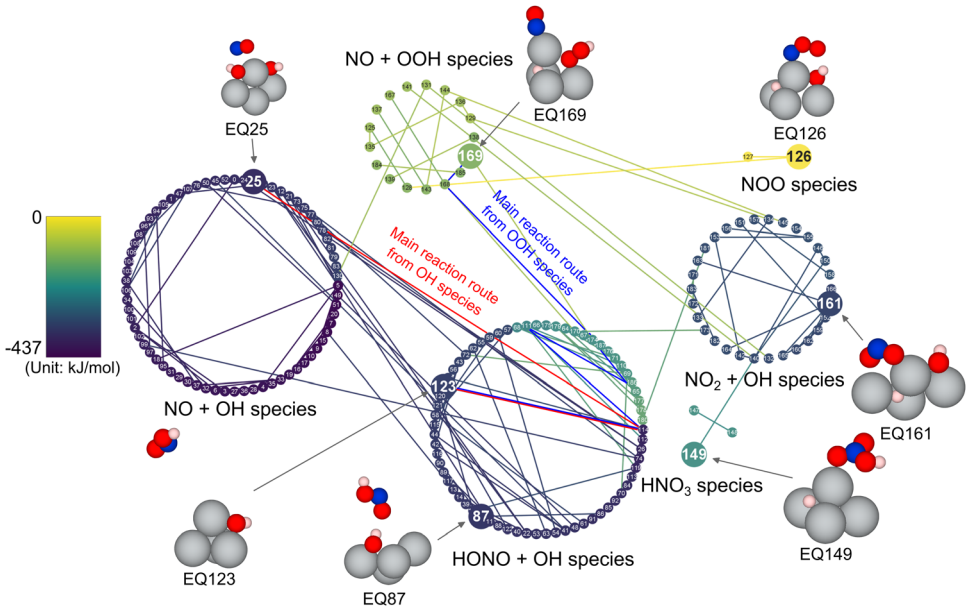

Fig. 4 Reaction route network for a NO molecule and $Ag_4(OH)_2$ in CHA zeolite (EQ21 in Fig. 2a). Nodes and edges describe obtained structures and paths connecting them (TS and PT, determined by GRRM program[16]). The color of the nodes and edges describes the relative energy (color bar is shown on the left side). The representative structures are displayed together (only Ag_4 cluster and reactants are shown for clarity).

dissociation (127 kJ mol^{-1} *vs.* 179 kJ mol^{-1}). These results indicated that the H_2 + O_2 mixture more facilely dissociates on the Ag_4 cluster than H_2O dissociation. The following section discusses the reactivity of OOH and OH species with NO molecules over the Ag_4 cluster.

3.2 Reactivity of OOH and OH species with a NO molecule to produce a HONO intermediate on a Ag_4 cluster

The reactivity of OOH and OH species previously formed on the Ag_4 cluster with an NO molecule was examined by the SC-AFIR method. One NO molecule was added to the structure of EQ21, as shown in Fig. 2a ($Ag_4(OH)_2$ species). Fig. 4 shows the results of the reaction route mapping, and Fig. 5a shows the relative energy along the main reaction route of the OH and NO molecules on the Ag_4 cluster. The adsorbed NO on the Ag_4 cluster reacted with OH species to form HONO species as a facile process (*Ea* = 13 kJ mol^{-1}). Subsequently, the formed HONO species was desorbed from the cluster *via* an *Ea* of 70 kJ mol^{-1}. With the same starting structure (EQ21 in Fig. 2a), the reaction of the OOH species and NO molecules was also explored. Fig. 5b shows the relative energies along the main reaction route for OOH + NO. To form the HONO species, the O–O bond in the OOH species was cleaved to provide an OH fragment, which subsequently reacted with adsorbed NO *via* an *Ea* of 47 kJ mol^{-1}. The formed HONO achieved the same structure as the case of OH species (EQ114) through relatively small *Ea*s (31 and 27 kJ mol^{-1}) before detaching through an *Ea* of 70 kJ mol^{-1} (EQ123). The formation of NO_2 species on the Ag_4 cluster was predicted as another reaction route from OOH + NO, and the evaluated *Ea* was low (17 kJ mol^{-1}). Our previous study demonstrated that N_2O_4 species, formed *via* the dimerization of NO_2, also produced NO^+ species at the Al site in the zeolite.[57] Besides, Bader charge analysis[78] was performed to evaluate the charge of the Ag_4 cluster before/after NO adsorption (Fig. S1, ESI†), and the result showed that the total charge of the cluster was not changed by NO adsorption while that of the NO molecule slightly decreased.

In summary, OH and OOH species, formed *via* the H_2 + O_2 reaction, easily oxidize NO to HONO or NO_2 species. Thus, H_2 addition promotes the formation of the highly active species OH and OOH on the Ag_4 cluster.

3.3 Reaction of NO + H_2 on the Ag_4 cluster toward NH_3 formation.

Three H_2 and one NO molecules were added to the periodic system, including the Ag_4 cluster (Fig. 1a), and reaction route mapping was carried out using the SC-AFIR method. Fig. 6 shows the reaction route for the $3H_2$ + NO reaction; the adsorbed NO was exothermically hydrogenated in a step-by-step manner to yield NH_3 and H_2O. Fig. 7 shows the energy profile along the main reaction route toward NH_3 and H_2O. First, the N atom of the adsorbed NO molecule is hydrogenated by the adjacent adsorbed H_2 molecule toward NH_2O species. This step has an exothermicity of 126 kJ mol^{-1} through a relatively high *Ea* (138 kJ mol^{-1}). Subsequently, the O atom in the formed NH_2O species was hydrogenated to give hydroxylamine (NH_2OH) and adsorbed H atoms with an *Ea* of 90 kJ mol^{-1}. Finally, the N–O bond in the formed NH_2OH is cleaved by the addition of H_2 molecules to give molecular NH_3 and H_2O with a high exothermicity (329 kJ mol^{-1}) through an *Ea* of 111 kJ mol^{-1}. The first process in the entire reaction pathway to give the NH_2O species exhibited the highest *Ea*. Considering the *Ea* for the formation of OH and OOH species

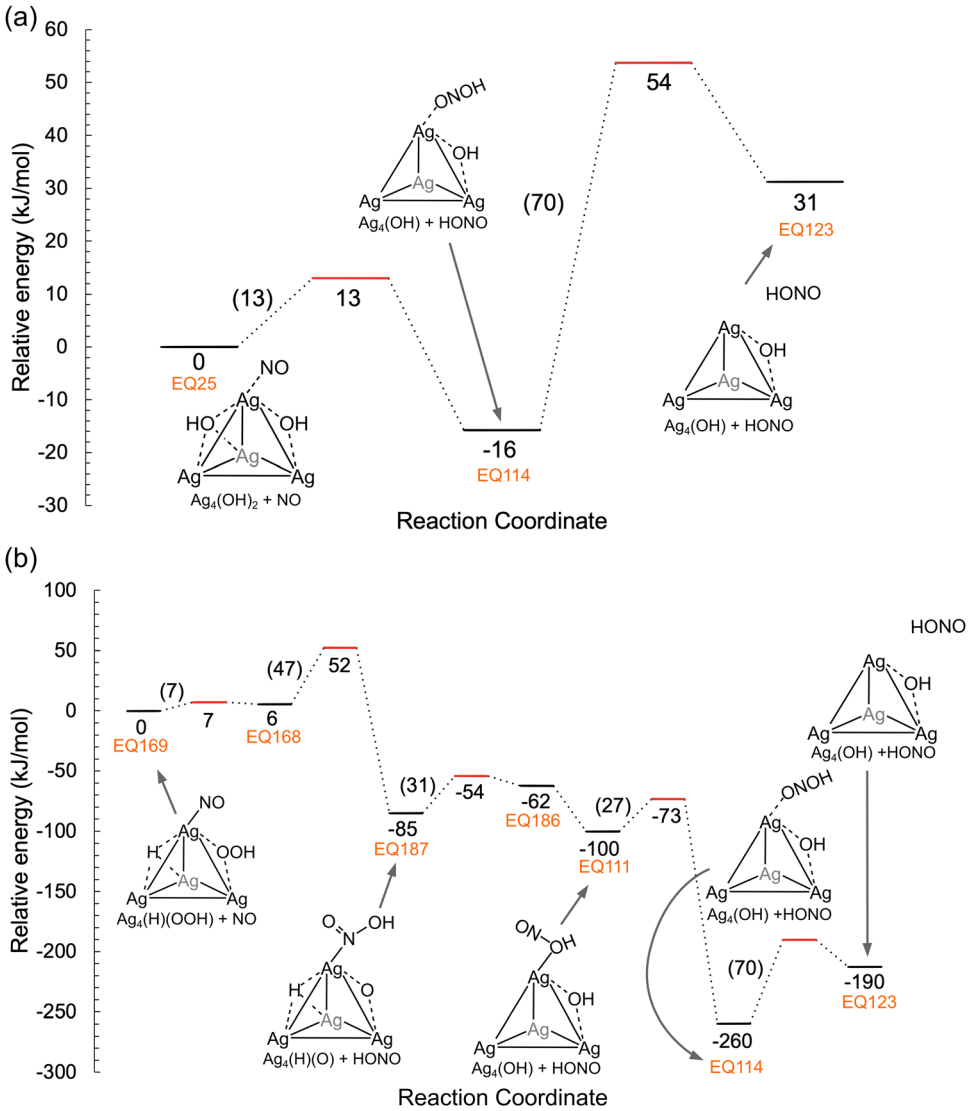

Fig. 5 Energy profile for the main reaction route toward EQ123 from (a) OH species and (b) OOH species. The relative energies of each structure and the activation barriers are shown below each bar and in brackets, respectively. A schematic view of the structures is displayed together.

(127 kJ mol^{-1}), the direct hydrogenation of NO with H_2 toward NH_3 is less plausible for the SCR reaction.

Fig. 8 shows the proposed reaction routes in this study, combined with previous reports.[56,57] In the presence of H_2 and O_2, OH and OOH species were generated on the Ag_4 cluster with an *Ea* of 127 kJ mol^{-1}. Moreover, the generation of OH species from adsorbed H_2O molecules required an *Ea* of 179 kJ mol^{-1}. The active species formed on the Ag_4 cluster, OH, and OOH species, easily reacted with the NO molecule to yield the HONO intermediate. As another possible reaction, the direct hydrogenation of NO with H_2 was assessed; the *Ea* for NH_3 formation was evaluated to be 138 kJ mol^{-1}, which is higher than that for the $H_2 + O_2$ reaction. The proposed contribution of H_2 addition to NH_3–SCR by zeolite-based catalysts is to boost the formation of active OH and OOH species on the Ag_4 cluster. Previous research on H_2-assisted SCR over Ag-loaded Al_2O_3 proposes that the main contribution of H_2 addition is stabilizing nitrate (NO_3^-) on the Al_2O_3 surface to prevent poisoning active Ag species, which is different from our result on zeolite-based catalysts.[40,42,45,79] For HC-SCR, the previous study using *in situ* spectroscopy proposed that C_3H_8 reacted with active species (*e.g.* OOH species) to form NH_3 (by the reaction with NO_2) through CH_3COO^-, CH_3NO_2, and NCO^- intermediates on the Ag_4 cluster.[52,55] According to this result, the formed HONO species is probably decomposed into N_2 and H_2O at Brønsted acid sites by the formed NH_3. Thus, the present study demonstrated the effective utilization of automated reaction route mapping to explore the reactions over multinuclear clusters confined in zeolites.

4. Conclusion

Automated reaction route mapping was carried out to explore the catalytic reaction over the Ag_4^{2+} cluster confined in the zeolite. The $H_2 + O_2$ reaction over the Ag_4^{2+} cluster indicated

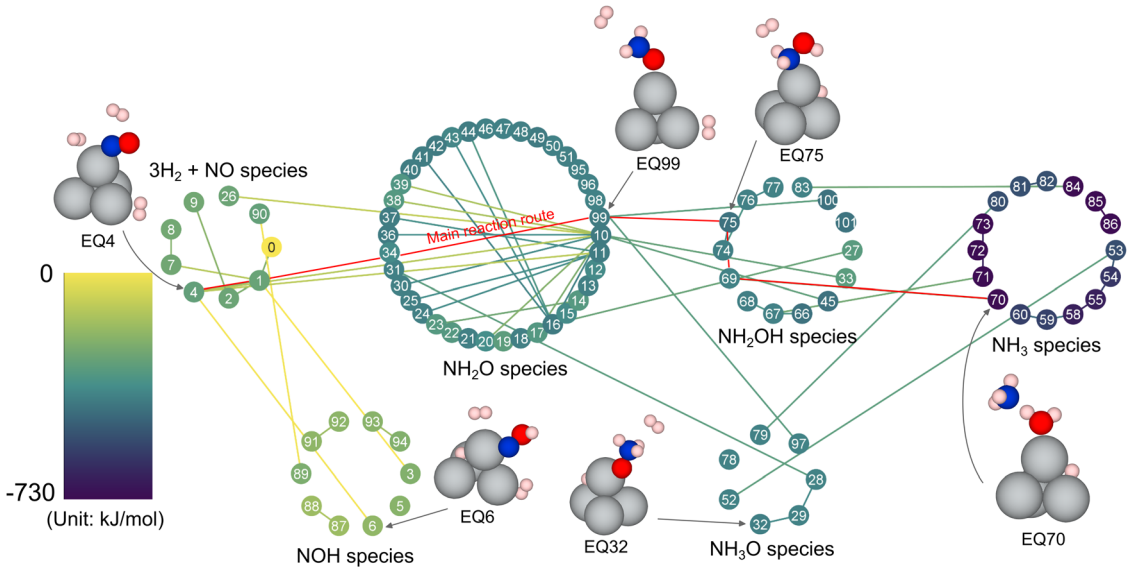

Fig. 6 Reaction route network for one NO and three H_2 molecules and the Ag_4 cluster in CHA zeolite. Nodes and edges describe obtained structures and paths connecting them (TS and path top (PT), determined by GRRM program[16]). The color of the nodes and edges describes the relative energy (color bar is shown on the left side). The representative structures are displayed together (only the Ag_4 cluster and reactants are shown for clarity).

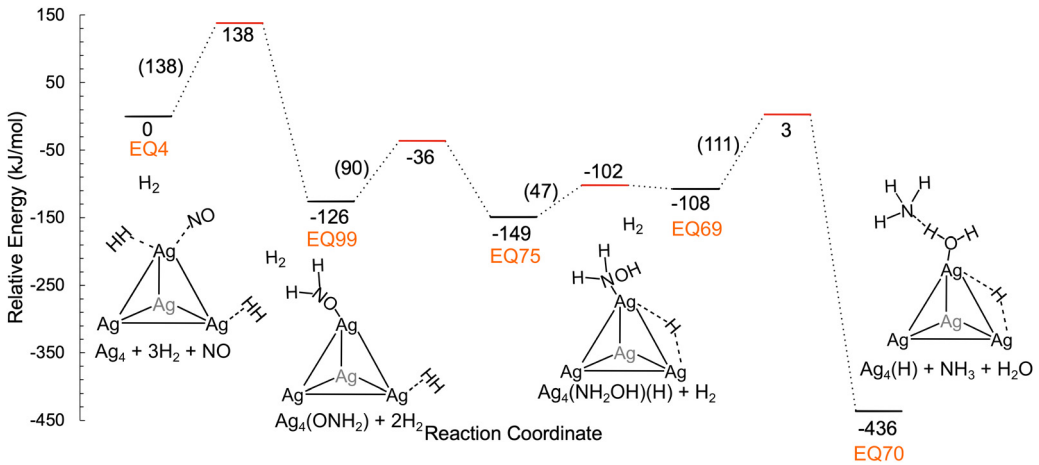

Fig. 7 Energy profile for the main reaction route (NO + $3H_2$ → NH_3 + H_2O + H) over the Ag_4 cluster. The relative energies of each structure and the activation barriers are shown below the bar and in brackets, respectively. A schematic view of the structures is displayed together.

that the generation of active species, OH and OOH species, required lower activation energy than that for the formation of OH species from the dissociative adsorption of H_2O (127 kJ mol^{-1} *vs.* 179 kJ mol^{-1}). The formed OH species were highly reactive with NO molecules to yield HONO species (*Ea* = 13 kJ mol^{-1}), whereas the reaction of NO and OOH species gave HONO or NO_2 species *via Ea*s of 47 and 17 kJ mol^{-1}, respectively. Additionally, the reactivity of H_2 with NO over the Ag_4 clusters was examined. This result revealed that the formation of NH_3 from NO + H_2 required an *Ea* as high as 138 kJ mol^{-1}, thus indicating that the NO molecule preferentially reacted with OH or OOH species formed on the Ag_4 cluster to give HONO. The present study demonstrated that the automated reaction route-searching method is suitable for investigating the catalytic reaction over multinuclear clusters with structural changes during the reaction.

Conflicts of interest

The authors declare no conflicts of interest.

Acknowledgements

This research was financially supported by the JST-CREST (JPMJCR17J3) and JSPS KAKENHI (21H04626). Some of the calculations were conducted employing the supercomputing resources at the Cyberscience Center of Tohoku University. This

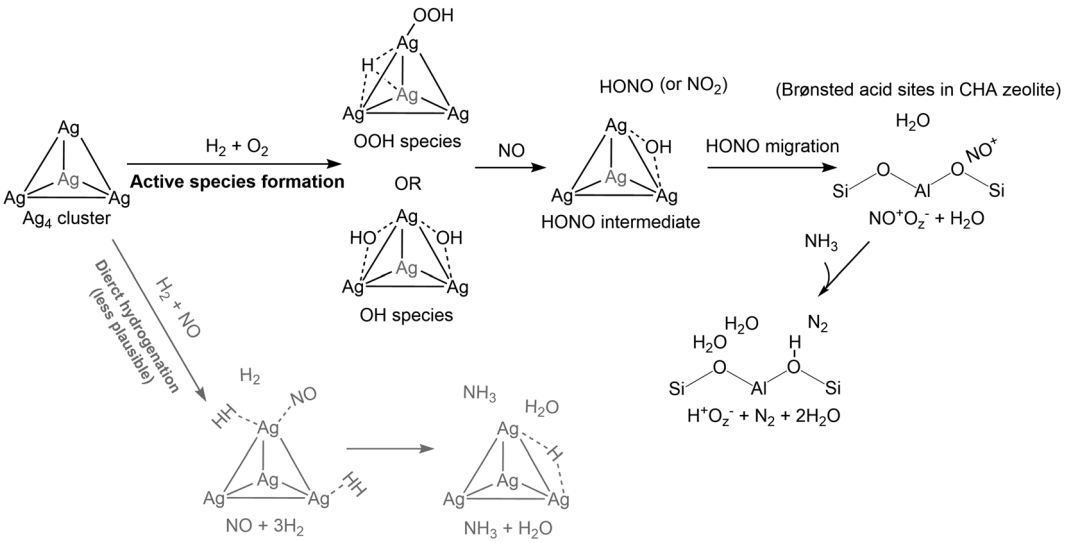

Fig. 8 Whole view of H_2-assisted NH_3–SCR over the Ag_4 cluster in CHA zeolite proposed in this study, combined with the reactions on Brønsted acid sites of CHA zeolite described in our previous reports.[57,75]

project was supported by the Joint Usage/Research Center for Catalysis. S.Y. is grateful to the MANABIYA system of the Institute for Chemical Reaction Design and Discovery (ICReDD) of Hokkaido University, which was established by the World Premier International Research Initiative (WPI), MEXT, Japan, to support the learning of the GRRM program techniques for DFT calculations. S.Y. acknowledges a Grant-in-Aid for JSPS Fellows (21J11744 (DC2)).

References

1 S. Stocker, G. Csányi, K. Reuter and J. T. Margraf, *Nat. Commun.*, 2020, **11**, 5505.
2 B. Kreitz, K. Sargsyan, K. Blöndal, E. J. Mazeau, R. H. West, G. D. Wehinger, T. Turek and C. F. Goldsmith, *JACS Au*, 2021, **1**, 1656–1673.
3 T. Lan and Q. An, *J. Am. Chem. Soc.*, 2021, **143**, 16804–16812.
4 J. Xu, X. M. Cao and P. Hu, *Phys. Chem. Chem. Phys.*, 2021, **23**, 11155–11179.
5 X. Fu, J. Li, J. Long, C. Guo and J. Xiao, *ACS Catal.*, 2021, **11**, 12264–12273.
6 R. T. Hannagan, G. Giannakakis, R. Réocreux, J. Schumann, J. Finale, Y. Wang, A. Michaelides, P. Deshlahra, P. Christopher, M. Flytzani-Stephanopoulous, M. Stamatakis and E. C. H. Sykes, *Science*, 2021, **372**, 1444–1447.
7 Z. W. Ulissi, A. J. Medford, T. Bligaard and J. K. Nørskov, *Nat. Commun.*, 2017, **8**, 14621.
8 A. A. Latimer, A. R. Kulkarni, H. Aljama, J. H. Montoya, J. S. Yoo, C. Tsai, F. Abild-Pedersen, F. Studt and J. K. Nørskov, *Nat. Mater.*, 2017, **16**, 225–229.
9 J.-M. Schweitzer, J. Rey, C. Bignaud, T. Bučko, P. Raybaud, M. Moscovici-Mirande, F. Portejoie, C. James, C. Bouchy and C. Chizallet, *ACS Catal.*, 2022, **12**, 1068–1081.
10 A. Bruix, J. T. Margraf, M. Andersen and K. Reuter, *Nat. Catal.*, 2019, **2**, 659–670.
11 K. Ohno and S. Maeda, *J. Phys. Chem. A*, 2006, **110**, 8933–8941.
12 S. Maeda, K. Ohno and K. Morokuma, *Phys. Chem. Chem. Phys.*, 2013, **15**, 3683–3701.
13 S. Maeda, T. Taketsugu, K. Ohno and K. Morokuma, *J. Am. Chem. Soc.*, 2015, **137**, 3433–3445.
14 S. Maeda, S. Komagawa, M. Uchiyama and K. Morokuma, *Angew. Chem., Int. Ed.*, 2011, **50**, 644–649.
15 S. Maeda, Y. Harabuchi, Y. Ono, T. Taketsugu and K. Morokuma, *Int. J. Quantum. Chem.*, 2015, **115**, 258–269.
16 S. Maeda, Y. Harabuchi, M. Takagi, K. Saita, K. Suzuki, T. Ichino, Y. Sumiya, K. Sugiyama and Y. Ono, *J. Comput. Chem.*, 2018, **39**, 233–250.
17 K. Sugiyama, Y. Sumiya, M. Takagi, K. Saita and S. Maeda, *Phys. Chem. Chem. Phys.*, 2019, **21**, 14366–14375.
18 S. Maeda, K. Sugiyama, Y. Sumiya, M. Takagi and K. Saita, *Chem. Lett.*, 2018, **47**, 396–399.
19 K. Sugiyama, K. Saita and S. Maeda, *J. Comput. Chem.*, 2021, **42**, 2163–2169.
20 M. Gao, A. Lyalin, M. Takagi, S. Maeda and T. Taketsugu, *J. Phys. Chem. C*, 2015, **119**, 11120–11130.
21 M. Gao, A. Lyalin, S. Maeda and T. Taketsugu, *J. Chem. Theory Comput.*, 2014, **10**, 1623–1630.
22 L. Liu, M. Lopez-Haro, J. A. Perez-Omil, M. Boronat, J. J. Calvino and A. Corma, *Nat. Commun.*, 2022, **13**, 821.
23 T. Yumura, A. Oda, H. Torigoe, A. Itadani, Y. Kuroda, T. Wakasugi and H. Kobayashi, *J. Phys. Chem. C*, 2014, **118**, 23874–23887.
24 Y. Chai, W. Shang, W. Li, G. Wu, W. Dai, N. Guan and L. Li, *Adv. Sci.*, 2019, **6**, 1900299.
25 S. Wu, X. Yang and C. Janiak, *Angew. Chem.*, 2019, **131**, 12468–12482.
26 S. Yasumura, M. Huang, X. Wu, C. Liu, T. Toyao, Z. Maeno and K. Shimizu, *Catal. Today*, 2020, **352**, 118–126.
27 Z. Maeno, S. Yasumura, C. Liu, T. Toyao, K. Kon, A. Nakayama, J. Hasegawa and K. Shimizu, *Phys. Chem. Chem. Phys.*, 2019, **21**, 13415–13427.

28 G. Li and E. A. Pidko, *ChemCatChem*, 2019, **11**, 134–156.
29 S. Grundner, M. A. C. Markovits, G. Li, M. Tromp, E. A. Pidko, E. J. M. Hensen, A. Jentys, M. Sanchez-Sanchez and J. A. Lercher, *Nat. Commun.*, 2015, **6**, 7546.
30 G. Li, P. Vassilev, M. Sanchez-Sanchez, J. A. Lercher, E. J. M. Hensen and E. A. Pidko, *J. Catal.*, 2016, **338**, 305–312.
31 M. H. Mahyuddin, A. Staykov, A. G. Saputro, M. K. Agusta, H. K. Dipojono and K. Yoshizawa, *J. Phys. Chem. C*, 2020, **124**, 18112–18125.
32 M. H. Mahyuddin, Y. Shiota, A. Staykov and K. Yoshizawa, *Acc. Chem. Res.*, 2018, **51**, 2382–2390.
33 M. H. Mahyuddin and K. Yoshizawa, *Catal. Sci. Technol.*, 2018, **8**, 5875–5885.
34 M. Gao, D. Horita, Y. Ono, A. Lyalin, S. Maeda and T. Taketsugu, *J. Phys. Chem. C*, 2017, **121**, 2661–2668.
35 T. Iwasa, T. Sato, M. Takagi, M. Gao, A. Lyalin, M. Kobayashi, K. Shimizu, S. Maeda and T. Taketsugu, *J. Phys. Chem. A*, 2019, **123**, 210–217.
36 J. P. Breen and R. Burch, *Top. Catal.*, 2006, **39**, 53–58.
37 K. Theinnoi, S. Sitshebo, V. Houel, R. R. Rajaram and A. Tsolakis, *Energy Fuels*, 2008, **22**, 4109–4114.
38 R. Bartolomeu, A. N. Mendes, A. Fernandes, C. Henriques, P. da Costa and M. F. Ribeiro, *Catal. Sci. Technol.*, 2016, **6**, 3038–3048.
39 F. Schuricht and W. Reschetilowski, *Microporous Mesoporous Mater.*, 2012, **164**, 135–144.
40 Y. Yu, H. He, X. Zhang and H. Deng, *Catal. Sci. Technol.*, 2014, **4**, 1239–1245.
41 F. Wang, G. He, B. Zhang, M. Chen, X. Chen, C. Zhang and H. He, *ACS Catal.*, 2019, **9**, 1437–1445.
42 G. Xu, H. Wang, Y. Yu and H. He, *J. Catal.*, 2021, **395**, 1–9.
43 P. S. Kim, M. K. Kim, B. K. Cho, I. S. Nam and S. H. Oh, *J. Catal.*, 2013, **301**, 65–76.
44 J. P. Breen, R. Burch, C. Hardacre, C. J. Hill, B. Krutzsch, B. Bandl-Konrad, E. Jobson, L. Cider, P. G. Blakeman, L. J. Peace, M. V. Twigg, M. Preis and M. Gottschling, *Appl. Catal. B*, 2007, **70**, 36–44.
45 S. Tamm, N. Vallim, M. Skoglundh and L. Olsson, *J. Catal.*, 2013, **307**, 153–161.
46 S. T. Korhonen, A. M. Beale, M. A. Newton and B. M. Weckhuysen, *J. Phys. Chem. C*, 2011, **115**, 885–896.
47 H. Kubota, S. Mine, T. Toyao, Z. Maeno and K. Shimizu, *ACS Catal.*, 2021, **3**, 544–559.
48 J. Shibata, K. Shimizu, S. Satokawa, A. Satsuma and T. Hattori, *Phys. Chem. Chem. Phys.*, 2003, **5**, 2154–2160.
49 J. Shibata, Y. Takada, A. Shichi, S. Satokawa, A. Satsuma and T. Hattori, *J. Catal.*, 2004, **222**, 368–376.
50 A. Satsuma, J. Shibata, K. Shimizu and T. Hattori, *Catal. Surv. Asia*, 2005, **9**, 75–85.
51 K. Shimizu, K. Sugino, K. Kato, S. Yokota, K. Okumura and A. Satsuma, *J. Phys. Chem. C*, 2007, **111**, 1683–1688.
52 K. Shimizu, K. Sawabe and A. Satsuma, *Catal. Sci. Technol.*, 2011, **1**, 331–341.
53 K. Sawabe, T. Hiro, K. Shimizu and A. Satsuma, *Catal. Today*, 2010, **153**, 90–94.
54 J. Shibata, K. Shimizu, Y. Takada, A. Shichi, H. Yoshida, S. Satokawa, A. Satsuma and T. Hattori, *J. Catal.*, 2004, **227**, 367–374.
55 K. Shimizu, K. Sugino, K. Kato, S. Yokota, K. Okumura and A. Satsuma, *J. Phys. Chem. C*, 2007, **111**, 6481–6487.
56 K. Shimizu and A. Satsuma, *Appl. Catal., B*, 2007, **77**, 202–205.
57 S. Yasumura, C. Liu, T. Toyao, Z. Maeno and K. Shimizu, *J. Phys. Chem. C*, 2021, **125**, 1913–1922.
58 G. Kresse and J. Furthmüller, *Phys. Rev. B: Condens. Matter Mater. Phys.*, 1996, **54**, 11169–11186.
59 G. Kresse and J. Furthmüller, *Comput. Mater. Sci.*, 1996, **6**, 15–50.
60 P. E. Blöchl, *Phys. Rev. B: Condens. Matter Mater. Phys.*, 1994, **50**, 17953–17979.
61 D. Kresse, G. Joubert, G. Kresse and D. Joubert, *Phys. Rev. B: Condens. Matter Mater. Phys.*, 1999, **59**, 1758–1775.
62 P. Honhenberg and W. Kohn, *Phys. Rev. [Sect.] B*, 1964, **136**, B864–B871.
63 W. Kohn and L. J. Sham, *Phys Rev A*, 1965, **140**, A1133–A1138.
64 J. P. Perdew, K. Burke and M. Ernzerhof, *Phys. Rev. Lett.*, 1996, **77**, 3865–3868.
65 H. J. Monkhorst and J. D. Pack, *Phys. Rev. B: Condens. Matter Mater. Phys.*, 1976, **13**, 5188–5192.
66 S. Grimme, S. Ehrlich and L. Goerigk, *J. Comput. Chem.*, 2011, **32**, 1456–1465.
67 S. Grimme, J. Antony, S. Ehrlich and H. Krieg, *J. Chem. Phys.*, 2010, **132**, 154104.
68 C. Baerlocher; L. B. McCusker; and H. van Koningsveld Database of Zeolite Structures; **http://www.iza-structure.org/databases/**(accessed Jun. 2021).
69 Z. Zhao, Y. Xing, S. Li, X. Meng, F. S. Xiao, R. McGuire, A. N. Parvulescu, U. Müller and W. Zhang, *J. Phys. Chem. C*, 2018, **122**, 9973–9979.
70 S. Yasumura, T. Ueda, H. Ide, K. Otsubo, C. Liu, N. Tsunoji, T. Toyao, Z. Maeno and K. Shimizu, *Phys. Chem. Chem. Phys.*, 2021, **23**, 22273–22282.
71 C. Paolucci, A. A. Parekh, I. Khurana, J. R. di Iorio, H. Li, J. D. Albarracin Caballero, A. J. Shih, T. Anggara, W. N. Delgass, J. T. Miller, F. H. Ribeiro, R. Gounder and W. F. Schneider, *J. Am. Chem. Soc.*, 2016, **138**, 6028–6048.
72 K. Fukui, *Acc. Chem. Res.*, 1981, **14**, 363.
73 S. Yasumura, K. Saita, T. Miyakage, T. Toyao, Z. Maeno, T. Taketsugu and K. Shimizu, *ChemRxiv*, 2022, preprint, DOI: **10.26434/chemrxiv-2022-w9fjz**.
74 S. Yasumura, Y. Qian, T. Toyao, Z. Maeno and K. Shimizu, *J. Phys. Chem. C*, 2022, **126**, 11082–11090.
75 S. Yasumura, Y. Qian, T. Kato, S. Mine, T. Toyao, Z. Maeno and K. Shimizu, *ACS Catal.*, 2022, **12**, 9983–9993.
76 H. Kubota, T. Toyao, Z. Maeno, Y. Inomata, T. Murayama, N. Nakazawa, S. Inagaki, Y. Kubota and K. Shimizu, *ACS Catal.*, 2021, **11**, 11180–11192.
77 C. Liu, S. Yasumura, T. Toyao, Z. Maeno and K. Shimizu, *J. Phys. Chem. C*, 2022, **126**, 11594–11601.
78 W. Tang, E. Sanville and G. Henkelman, *J. Phys.: Condens. Matter*, 2009, **21**, 084204.
79 G. Xu, J. Ma, L. Wang, Z. Lv, S. Wang, Y. Yu and H. He, *ACS Catal.*, 2019, **9**, 10489–10498.